Analytical Methods

Accepted Manuscript

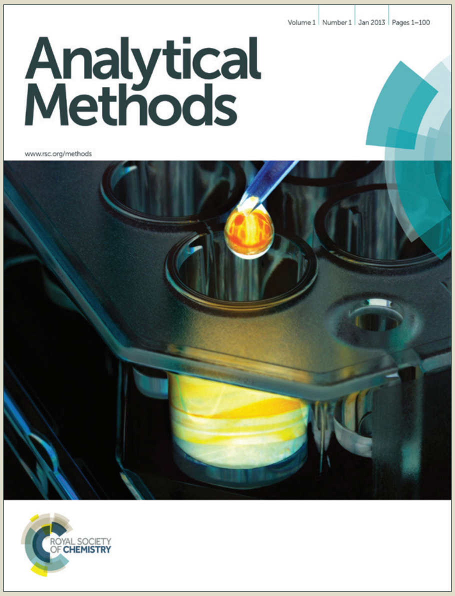

Volume 1 | Number 1 | Jan 2013 | Pages 1–100

Analytical Methods

www.rsc.org/methods

ROYAL SOCIETY OF CHEMISTRY

ROYAL SOCIETY OF CHEMISTRY

www.rsc.org/methods

Analytical Methods

ARTICLE

The Performance of a Nitrogen-Containing Tetrahedral Amorphous Carbon Electrode in Flow Injections Analysis with Amperometric Detection

Received 00th January 20xx,
Accepted 00th January 20xx

DOI: 10.1039/x0xx00000x

www.rsc.org/

D'Nisha Hamblin[a], Joy Qiu[a,b], Lars Haubold[c] and Greg M. Swain[a]

*Corresponding author: email. swain@chemistry.msu.edu

Abstract

The performance of a nitrogen-incorporated tetrahedral amorphous (t*a*-C:N) carbon thin-film electrode was evaluated using flow injection analysis with amperometric detection. The response stabilization time, and background current and noise were evaluated as a function of the applied potential. The analytical detection figures of merit for norepinephrine in 0.1 M phosphate buffer (pH 7.2) were also determined for the t*a*-C:N electrode and compared with values obtained at a boron-doped nanocrystalline diamond film electrode. The t*a*-C:N electrode exhibited more rapid stabilization times, and lower background current and noise at all potentials from 0.1 to 0.9 V vs. Ag/AgCl. The response precision, sensitivity, linear dynamic range and limit of detection were as good or superior for the t*a*-C:N electrode. The results portend the analytical utility of this new carbon electrode material.

Introduction

In electroanalytical measurements using sp^2 carbon electrodes, particularly amperometric detection coupled with flow injection analysis or liquid chromatography, the microstructural stability of the electrode becomes an issue when used at positive potentials. Generally, at potentials positive of 0.5 V vs. Ag/AgCl in acid, microstructurally-disordered sp^2 carbons undergo surface oxidation reactions that lead to increased background current in amperometric detection due to increased pseudocapacitance and surface roughening. At more positive potentials, approximately ≥ 0.8 V, more extensive microstructural alterations, surface roughening and even carbon corrosion can occur. The carbon corrosion reaction can be written as follows:

$$C + 2H_2O \rightarrow CO_2 + 4H^+ + 4e^-$$

All of these processes will lead to unstable and even increasing background current and noise with time. This drift progressively reduces the signal-to-background (S/B) and signal-to-noise (S/N) ratios in amperometric measurements. The concept is depicted in Figure 1.

Boron-doped diamond electrodes have been researched for some 20 years now (1-4). These electrodes offer some unique properties, as compared to conventional sp^2 carbon electrodes, such as (i) a low and stable background current (5-10x lower that a polished glassy carbon electrode of the same geometric area) that leads to enhanced signal-to-background ratios in electroanalytical measurements, (ii) a wide potential window that enables measurements of analytes that require extreme positive or negative potentials for detection (e.g., oxidative detection of azide) (5), (iii) relatively rapid electron-transfer kinetics for a number of redox systems without conventional carbon electrode pretreatment (k^o_{app} ~0.01-0.1 cm/s) (6,7), (iv) weak molecular adsorption and

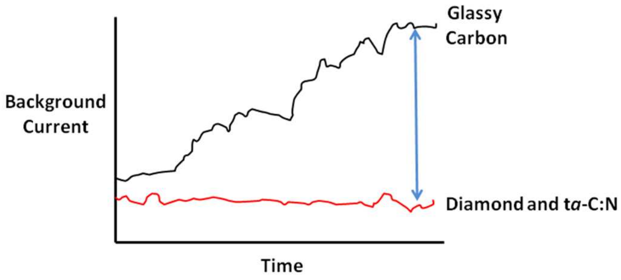

Figure 1. Hypothetical background current –time response for a glassy carbon, a diamond and a nitrogen-incorporated tetrahedral amorphous carbon (t*a*-C:N) electrode at a positive detection potential where the former electrode undergoes surface oxidation, microstructural alterations and even carbon corrosion.

---

[a] *Department of Chemistry, Michigan State University, East Lansing, MI 48824*
[b] *High School Honors Science Program(HSHP), Michigan State University, East Lansing, MI 48824*
[c] *Center for Coatings and Diamond Technology, Michigan State University, East Lansing, MI 48824.*
† Footnotes relating to the title and/or authors should appear here.
Electronic Supplementary Information (ESI) available: [details of any supplementary information available should be included here]. See DOI: 10.1039/x0xx00000x

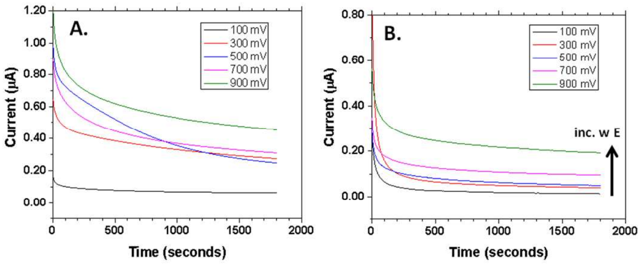

Figure 2. Background current-time profiles for (A) a boron-doped nanocrystalline diamond and (B) a t*a*-C:N thin-film electrode as a function of the applied potential. Measurements were made in the thin-layer flow cell in 0.1 M phosphate buffer (pH 7.2). Flow rate = 0.5 mL/min.

resistance to electrode fouling (8) and (v) good microstructural stability during the imposition of high currents and potentials. This latter property gives rise to the stable background current with time as depicted in Figure 1.

Despite these excellent properties, a disadvantage of diamond is the rather high deposition temperature required for growth, 600-800 °C. This limits the types of substrates that can be coated. It has been observed that nitrogen-incorporated tetrahedral amorphous carbon (t*a*-C:N) thin-film electrodes offer many of the same properties as boron-doped diamond, but they can be deposited near room temperature (9-12).

The t*a*-C:N electrode is one of three new types of mixed microstructure (sp^2-sp^3) carbon electrodes that exhibit properties similar to those of conducting diamond. Some of the basic electrochemical properties of these electrodes were first reported by the Miller group back in the late 1990's (9,10). Electroanalytical applications have not yet been extensively reported on for this electrode. Recently, though, a more detailed description of the structure and electrochemical properties of these electrodes has been published (12) and one report has demonstrated its use for the electrochemical detection of propranolol and hydrochlorothiazide (13). This electrode, which consists of a mixture of sp^2- and sp^3-bonded carbon, exhibits electrochemical properties very similar to those of diamond: low background current, wide working potential window, relatively rapid electron-transfer kinetics for several inorganic redox systems without conventional pretreatment, weak molecular adsorption (e.g., methylene blue) and microstructural stability. This latter property gives rise to a stable background current, as is depicted in Figure 1. The electrical resistance of the t*a*-C film decreases with increasing nitrogen incorporation (12). The ratio of sp^2-to-sp^3-bonded carbon also increases with increasing nitrogen incorporation (12). The film used in this work had an sp^3/sp^2 carbon ratio of ca. 0.40 and an electrical resistivity of ca. 0.01 ohm-cm.

Two other "diamond-like" carbon electrodes that exhibit electrochemical properties similar to those of boron-doped diamond are the nanocarbon films being studied by the Niwa group that are formed by electron cyclotron resonance sputtering (14-17) and the amorphous carbon nitride (a-CNx) films being investigated by Deslouis and co-workers (18-23). The latter films are deposited by DC magnetron sputtering and can be formed as a pin-hole free thin film. The nanocarbon films are atomically flat, highly conductive and possess an sp^3/sp^2 carbon ratio of ca. 0.70 (14-17).

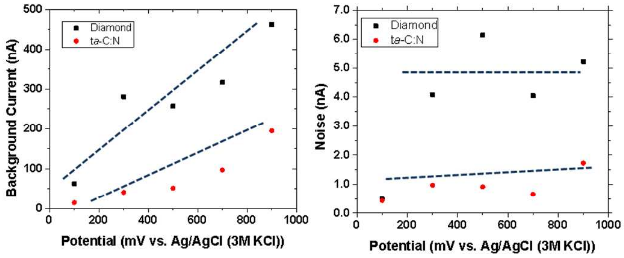

Figure 3. Plots of the mean background current (left) and noise (right) for a boron-doped nanocrystalline diamond and a t*a*-C:N thin-film electrode as a function of the applied potential. Measurements were made in the thin-layer flow cell in 0.1 M phosphate buffer (pH 7.2). Flow rate = 0.5 mL/min. The dashed lines have no statistical significance and are included to orient the reader on the data trends.

In this work, we report on the electroanalytical performance of a nitrogen-incorporated tetrahedral amorphous (t*a*-C:N) carbon film in flow injection analysis with amperometric detection. The response stabilization time, and background current and noise were evaluated as a function of the applied potential. The analytical detection figures of merit for norepinephrine in 0.1 M phosphate buffer (pH 7.2) were also determined for the t*a*-C:N electrode and compared with values obtained at a boron-doped nanocrystalline diamond film electrode.

Experimental Methods

ta-C:N Electrode Preparation. The t*a*-C:N film was grown on a boron-doped Si (111) substrate (Virginia Semiconductor, Fredericksburg, VA; ~10^{-3} Ω-cm) using pulsed laser-arc deposition (Laser-Arco system) at the Center for Coatings and Diamond Technology at Michigan State University . The Laser-Arc® technology combines the advantages of pulsed laser deposition and vacuum arc deposition processes. This system works by laser-controlled, high pulsed-current cathodic vacuum arc deposition (24,25). In the process, a pulsed laser beam is rastered across a rotating graphite target (cathode) that is positioned near the substrate. The laser combined with an optical scanner defines the location of each discharge for maximum graphite target utilization. Each laser pulse generates a small carbon-containing plasma that rapidly expands away from the metal anode toward the substrate. Once the conducting plasma reaches the substrate, a vacuum arc discharge is ignited between the target (graphite) and the substrate with peak currents approaching 1500 A. This deposition method produces thin, hard, and dense t*a*-C films. The substrate-target distance was approximately 12 cm. Carbon particles are produced during the arc evaporation process and these species serve as the growth precursors for the film (25). The nitrogen-incorporated films were deposited in the presence of nitrogen gas at a flow rate of 30 sccm (t*a*-C:N). The pulse duration was 0.33 msec, pulse frequency was 500 Hz and the deposition rate approached 6 μm/h. The deposition chamber was under high vacuum (< 10^{-5} mbar) except when N_2 gas was added. The substrate temperature during deposition was < 100 °C. The film had a thickness in the range of 200-400 nm, as determined by a Dektak profilometer, and an atomic nitrogen level of ca. 8-10%, as determined by auger electron spectroscopy depth profiling.

The boron-doped nanocrystalline diamond film was deposited by microwave-assisted chemical vapor deposition using a 1% CH_4/H_2

source gas ratio with 10 ppm of B_2H_6 added for the boron doping. The doping level was in the low 10^{21} cm^{-3} range leading to a resistivity of 0.01 ohm-cm. The nominal grain size was ca. 500 nm.

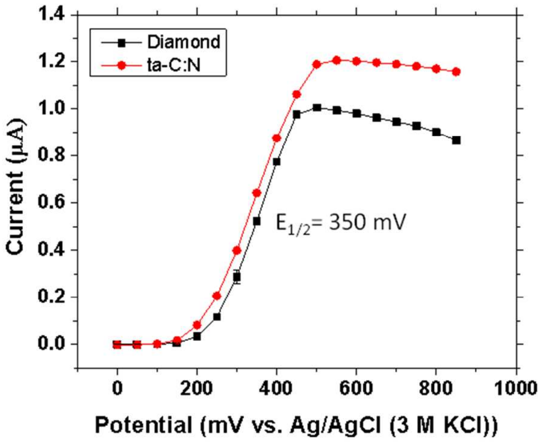

Figure 4. Hydrodynamic voltammograms for 100 μM norepinephrine in 0.1 M phosphate buffer (pH 7.2) at a boron-doped nanocrystalline diamond and a t*a*-C:N thin-film electrode. Flow rate = 0.5 mL/min. Injection volume = 25 μL.

Flow Injection Analysis. The thin-layer flow cell and the flow injection analysis system have been described elsewhere (26). The mobile phase was regulated with a Alltech Model 301 HPLC pump (Grace), through a Model 7125 injection value (Rheodyne) with a 25 μL injection loop and into a home-built, thin-layer flow cell. The flow cell was of the cross-flow type. The system possessed inert gas purge capability. A Model LP-21 pulse dampener (Scientific Systems) was placed in series between the pump and the injection valve. The entire system was grounded and the flow cell was placed inside a Faraday cage for shielding. The thin-layer flow cell was constructed with two pieces of Kel-f. The top piece contained the entrance and exit ports for the carrier solution and a place for the no-leak Ag/AgCl reference electrode (Dionex). The exit port was fitted with a short piece of stainless steel tubing (~6 cm in length) that served as the counter electrode. The bottom piece supported the t*a*-C:N working electrode. Electrical contact was made by pressing a piece of copper foil against the back side of the conducting Si substrate. To make ohmic contact, the oxide layer was removed by polishing. The polishing debris removed with a cotton swab and some alcohol, and the surface was then covered with a layer of graphite from a pencil. A 0.1 cm thick neoprene rubber gasket separated the surface of the working electrode from the top piece of the cell. A rectangular groove (1.1 cm x 0.1 cm x 0.1 cm) was cut into the gasket, which defined the flow channel. Assuming a 25% compression of the gasket when the two pieces of the cell are clamped together, the cell volume is estimated to be on the order of 10 μL.

Potentials were controlled and currents measured using a Model 832A electrochemical workstation (CH Instruments, Austin, TX). The carrier solution was 0.1 M phosphate buffer (pH 7.2) prepared with an equimolar mixture of potassium phosphate monobasic (KH_2PO_4, Jade Scientific) and potassium phosphate dibasic (K_2HPO_4, Columbus Chemical Industries). The norepinephrine (Sigma) solutions were prepared in the phosphate buffer. All solutions were prepared with ultrapure water (~18 Mohm-cm) from a Barnstead E-Pure system (deionized and passed over activated carbon).

Results and Discussion

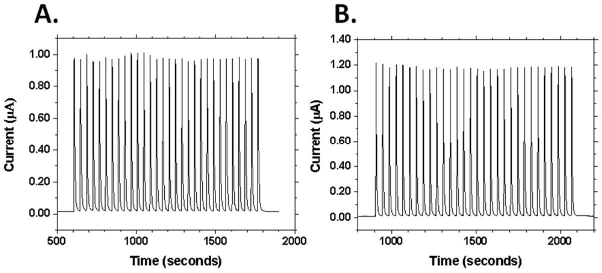

Figure 5. Repeated injections (30) of 100 μM norepinephrine in 0.1 M phosphate buffer (pH 7.2) at (A) a boron-doped nanocrystalline diamond and (B) a t*a*-C:N thin-film electrode. Flow rate = 0.5 mL/min. Injection volume = 25 μL.

Figure 2A and B shows background current-time profiles for a boron-doped nanocrystalline diamond film and a t*a*-C:N film electrode after the application of different potentials from 0.1 to 0.9 V vs. Ag/AgCl. The measurements were made using a 0.1 M phosphate buffer (pH 7.2) carrier solution at a flow rate of 0.5 mL/min. Figure 1A shows the response for a boron-doped diamond thin-film electrode. The current at the end of the 30 min period increases with the potential as expected. At the low potential, the background current stabilizes quickly, however, at the higher potentials a completely stable current is not quite achieved within the 30 min period. In contrast, the background current for the t*a*-C:N electrode is lower than the current for the diamond electrode at all potentials and the currents stabilize within the first 200-300 s. The rapid stabilization time is an attribute of this electrode for electroanalysis at all potentials.

Figure 3A and B show plots of the mean background current recorded at the end (last 5 min) of the 30-min potential step period and the noise (standard deviation about the mean) for the boron-doped diamond and t*a*-C:N electrodes. It is clear that the magnitude of the background current for both electrodes increases with the potential but the currents for the t*a*-C:N electrode are lower than those for the diamond electrode by a factor of 3-4x, particularly at the higher potentials. It is also clear that the noise for both electrodes is independent of the potential with the noise for the t*a*-C:N electrode being a factor of 5x lower at all potentials. This means that these electrodes offer an inherent advantage in S/B and S/N ratios as compared to diamond, which is superior to glassy carbon.

Figure 4 shows hydrodynamic voltammograms for 100 μM norepinephrine in 0.1 M phosphate buffer (pH 7.2) at the boron-doped nanocrystalline diamond and the t*a*-C:N electrode. The flow rate was 0.5 mL/min and the injection volume was 25 μL. The data reveal that the t*a*-C:N electrode exhibits a half-wave potential, $E_{1/2}$, that is the same as that for the boron-doped diamond electrode. The $E_{1/2}$ value is 350 mV. This result indicates that the t*a*-C:N electrode exhibits similar activity for this analyte as does diamond. Importantly, the curves for both electrodes were obtained without any conventional pretreatment other than flowing a small volume of ultrapure isopropanol across the electrode prior to recording the

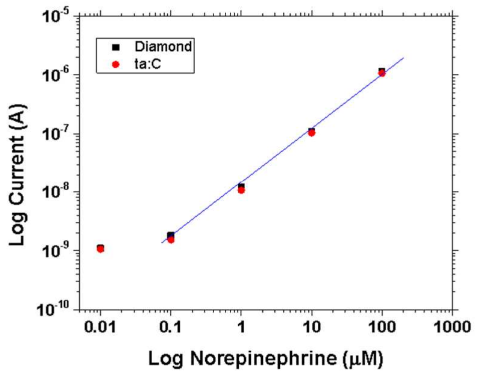

Figure 6. Response curves for norepinephrine in 0.1 M phosphate buffer (pH 7.2) at a boron-doped nanocrystalline diamond and a t*a*-C:N thin-film electrode. Flow rate = 0.5 mL/min. Injection volume = 25 μL.

hydrodynamic voltammograms. The t*a*-C:N electrode exhibits a slightly higher steady-state current because the height of the flow channel was different for the two electrodes due to differences in tightness of the cell (i.e., how compressed the thin-layer gasket was). Generally, the steady-state currents for both electrode types are the same in the FIA analysis.

Figure 5 presents reproducibility data for 25 μL injections of 100 μM norepinephrine in 0.1 M phosphate buffer (pH 7.2) at the boron-doped nanocrystalline diamond and the t*a*-C:N electrode. Thirty injections were made at a detection potential of 0.550 V. The results demonstrate that the t*a*-C:N electrode provides as good short-term response reproducibility as does the diamond electrode. The relative standard deviation of the peak height was 1.50% for diamond and 1.25% for t*a*-C:N, both of which are superior to glassy carbon (typically 5-10%). The response reproducibility is the most critical figure of merit when one is designing a new electrochemical assay and clearly the t*a*-C:N electrode provides superb reproducibility.

Figure 6 shows response curves for the two electrodes to different injected concentrations of norepinephrine. Replicate measurements were made (n=3). Error bars are within the size of the marker due to the high response reproducibility of both electrodes. The response curves for both electrodes are essentially the same with good linearity over four orders of magnitude ($r^2 > 0.998$) from 0.1 to 100 μM. The lowest injected concentration that could be detected was 0.1 nM (S/N > 3). The lower limit of detection actually falls between 10 and 100 μM for both electrodes. Table 1 summarizes the detection figures of merit for the two electrodes. Clearly, the detection figures of merit are nearly identical for the two electrodes.

Conclusions

The analytical performance of a t*a*-C:N thin-film electrode in amperometric detection coupled with flow injection analysis was studied. The response stabilization time, and background current and noise were evaluated as a function of the applied potential. The analytical detection figures of merit for norepinephrine in 0.1 M phosphate buffer (pH 7.2) were also determined for the t*a*-C:N electrode and compared with values obtained at a boron-doped nanocrystalline diamond film electrode. The t*a*-C:N electrode exhibited more rapid stabilization times, and lower background current and noise at all potentials from 0.1 to 0.9 V vs. Ag/AgCl. The response precision, sensitivity, linear dynamic range and limit of detection were as good or superior for the t*a*-C:N electrode. The results portend the analytical utility of this new carbon electrode material.

Table 1. Detection figures of merit for norepinephrine at a boron-doped diamond and a t*a*-C:N thin-film electrode.

Detection Figure of Merit	Boron-Doped Nanocrystalline Diamond	t*a*-C:N
Sensitivity (nA/μM)	11.4	10.7
Linear Dynamic Range (μM)	0.1 to 100	0.1 to 100
Reproducibility (coefficient of variance)	1.50%	1.25%
Limit of Detection (nM, S/N ≥ 3)	10-100	10-100

Acknowledgements

This work was supported by grants from the Army Research Office (W911NF-12-R-0011) and the National Science Foundation (CHE-0911383). Any opinions, findings, and conclusions or recommendations expressed in this paper are those of the authors and do not necessarily reflect the views of the funding agencies (ARO and NSF). The authors thank Dr. Wayne Jennings of the Swagelok Center for Materials Characterization at Case Western Reserve University for the auger electron spectroscopic measurements of the t*a*-C films.

References

1. G. M. Swain and R. Ramesham, *Anal. Chem*. 1993, **65**, 345.
2. T. N. Rao and A. Fujishima, *Diam. Rel. Mater*. 1999, **9**, 384.
3. M. Hupert, A. Muck, J. Wang, J. Stotter, Z. Cvackova, S. Haymond, Y. Show and G. M. Swain, *Diam. Rel. Mater*. 2003, **12**, 1940.
4. T. Watanabe, Y. Honda, K. Kanada and Y. Einaga, *Phys. Stat. Sol. A – Appl. Mater. Sci.* 2014, **211**, 2709.
5. J. Xu and G. M. Swain, *Anal. Chem*. 1998, **70**, 1502.
6. M. C. Granger, M. Witek, J. Xu, J. Wang, M. Hupert, A. Hanks, M. D. Koppang, J. E. Butler, G. Lucazeau, M. Mermoux, J. W. Strojek and G. M. Swain, *Anal. Chem.* 2000, **72**, 3523.
7. A. E. Fischer, Y. Show and G. M. Swain, *Anal. Chem*. 2004, **76**, 2553.
8. J. S. Xu, Q. Y. Chen, G. M. Swain, *Anal. Chem*. 1998, 70, 3146.
9. N. Vinokur, B. Miller, Y. Avygigal and R. Kalish, *J. Electrochem. Soc*. 1996, **143**, L238.
10. K. Yoo, B. Miller, R. Kalish and X. Shi, *Electrochem. Solid-State Lett.* 1999, **2**, 233.
11. A. Zeng, V. F. Neto, J. J. Gracio and Q. H. Fan, *Diam. Rel. Mater*. 2014, **43**, 12.
12. X. Yang, L. Haubold, G. DeVivo and G. M. Swain, *Anal. Chem*. 2012, **84**, 6240.

13. B. Lourencao, T. A. Silva, O. Fatibello-Filho and G. M. Swain, *Electrochim. Acta* 2014, **143**, 398.
14. T. Kamata, D. Kato, S. Hirono and O, Niwa, *Anal. Chem*. 2013, **85**, 9485.
15. N. Selioka, D. Kato, A. Ueda, T. Kamata, R. Kurita, S. Umemura, S. Hirono and O. Niwa, *Carbon* 2008, **46**, 1918.
16. J. Jia, D. Kato, R. Kurita, Y. Sato, K. Maruyama, K. Suzuki, S. Hirono, T. Ando and O. Niwa, *Anal. Chem* 2007, **79**, 98.
17. O. Niwa, J. Jia, D. Kato, R. Kurita, K. Maruyama, K. Suzuki, and S. Hirono, *J. Am. Chem. Soc*. 2006, **128**, 144.
18. A. Benchikh, C. Debiemme-Chouvy, H. Cachet, A. Palleret, B. Saidini, L. Beaunier, M. H. Berger and C. Deslouis, *Electrochim. Acta* 2012, **75**, 131.
19. H. Cachet, C. Debiemme-Chouvy, C. Deslouis, A. Lagrini, V. Vivier, *Surf. Interfaces Anal.* 2006, **38**, 719.
20. H. Cachet, C. Debiemme-Chouvy, C. Deslouis, A. Lagrini, V. Vivier, M. Benlahasen and S. Charvet, *Electrochem. Comm*. 2005, **7**, 496.
21. A. Lagrini, S. Charvet, M. Benlahasen, C. Debiemme-Chouvy, C. Deslouis and H. Cachet, *Thin Solid Films* 2005, **482**, 41.
22. A. Lagrini, C. Deslouis, H. Cachet, M. Benlahasen and S. Charvet, *Electrochem. Comm.* 2004, **6**, 245.
23. H. Cachet, C. Deslouis, M. Chouiki, B. Saidani, M. J. N. Conway, C. Godet, *J. Electrochem. Soc.* 2002, **149**, E233.
24. B. Kleinsorge, A. C. Ferrari, J. Robertson and W. I. Milne, *J. Appl. Phys.* 2000, **88**, 1149.
25, D. Drescher, J. Koskinen, H.-J. Scheibe and A. Mensch, *Diam. Rel. Mater.* 1998, **7**, 1375.
26. S. Jolley, M. Koppang, T. Jackson and G. M. Swain, *Anal. Chem.* 1997, **9**, 4099.